

Altering the Electrostatic Potential in the Major Groove: Thermodynamic and Structural Characterization of 7-Deaza-2'-deoxyadenosine:dT Base Pairing in DNA

Ewa A. Kowal,[†] Manjori Ganguly,[‡] Pradeep S. Pallan,[§] Luis A. Marky,^{||} Barry Gold,[‡] Martin Egli,[§] and Michael P. Stone^{*,†,§}

[†]Department of Chemistry, Vanderbilt University, Nashville, Tennessee 37235, United States

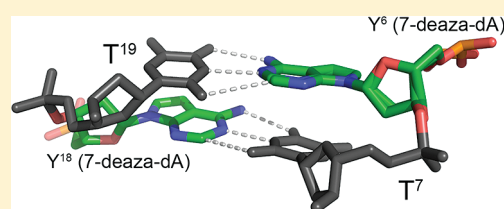
[‡]Department of Pharmaceutical Sciences, University of Pittsburgh, Pittsburgh, Pennsylvania 15261, United States

[§]Department of Biochemistry, Vanderbilt University, Nashville, Tennessee 37232, United States

^{||}Department of Pharmaceutical Sciences, University of Nebraska Medical Center, Omaha, Nebraska 68198, United States

Supporting Information

ABSTRACT: As part of an ongoing effort to explore the effect of major groove electrostatics on the thermodynamic stability and structure of DNA, a 7-deaza-2'-deoxyadenosine:dT (7-deaza-dA:dT) base pair in the Dickerson–Drew dodecamer (DDD) was studied. The removal of the electronegative N7 atom on dA and the replacement with an electropositive C–H in the major groove was expected to have a significant effect on major groove electrostatics. The structure of the 7-deaza-dA:dT base pair was determined at 1.1 Å resolution in the presence of Mg²⁺. The 7-deaza-dA, which is isosteric for dA, had minimal effect on the base pairing geometry and the conformation of the DDD in the crystalline state. There was no major groove cation association with the 7-deaza-dA heterocycle. In solution, circular dichroism showed a positive Cotton effect centered at 280 nm and a negative Cotton effect centered at 250 nm that were characteristic of a right-handed helix in the B-conformation. However, temperature-dependent NMR studies showed increased exchange between the thymine N3 imino proton of the 7-deaza-dA:dT base pair and water, suggesting reduced stacking interactions and an increased rate of base pair opening. This correlated with the observed thermodynamic destabilization of the 7-deaza-dA modified duplex relative to the DDD. A combination of UV melting and differential scanning calorimetry experiments were conducted to evaluate the relative contributions of enthalpy and entropy in the thermodynamic destabilization of the DDD. The most significant contribution arose from an unfavorable enthalpy term, which probably results from less favorable stacking interactions in the modified duplex, which was accompanied by a significant reduction in the release of water and cations from the 7-deaza-dA modified DNA.



INTRODUCTION

Nucleoside analogs containing pyrrolopyrimidine bases,^{1,2} or 7-deazapurines, are used as isosteric analogs of adenine and guanine in biochemical and biophysical studies.^{3–7} The 7-deazapurines are also used to study the effects of site-specific alteration of the electrostatic potential of the DNA major groove, where it has been shown for 7-deazaguanine that there is a significant alteration in DNA hydration and cation binding.^{7,8} The 7-deazaadenosine base was identified in the antibiotic tubercidin, a ribonucleoside isolated from various species of *Streptomyces*.^{2,9–11} The incorporation of 7-deaza-dA into DNA hinders the processing of the double helix by proteins, e.g., restriction endonucleases.¹² It slightly reduces the bending of DNA in oligodeoxynucleotides containing d(GGCA₆C)·d(CCGT₆G) tracts.^{13,14} The preparation of phosphoramidites containing 7-deaza-dA has been described by Seela et al.^{15,16}

There remains a paucity of quantitative data as to how substitution of adenine with 7-deaza-dA alters the structure and thermodynamics of the DNA double helix. Thermal denaturation of (7-deaza-dA)₁₁A·T₁₂ as compared to dA₁₂·dT₁₂ led to the conclusion that destabilization induced by 7-deaza-dA was

associated with an unfavorable entropy change.¹⁷ Pope et al.¹⁸ conducted a high-angle X-ray fiber diffraction study of poly[d(7-deaza-dA-T)]·poly[d(7-deaza-dA-T)]. They suggested that replacement of dA by 7-deaza-dA caused slight alterations to the structure of A-DNA, but greater perturbations to B-DNA. When 7-deaza-dG was incorporated into the Dickerson–Drew dodecamer (DDD)^{19,20} it had minimal effect on the overall conformation determined by NMR or crystallography.^{7,21} However, duplex stability was reduced adjacent to the modification site due to a loss of enthalpic stabilization. Moreover, 7-deaza-dG caused a reduction in hydration and cation binding. This was attributed to the elimination of a high affinity major groove cation binding site.²¹ Clearly, while 7-deaza-dG was an isostere of dG, it altered the ensemble of DNA, water and salts, and thermodynamic stability of the DDD.⁷

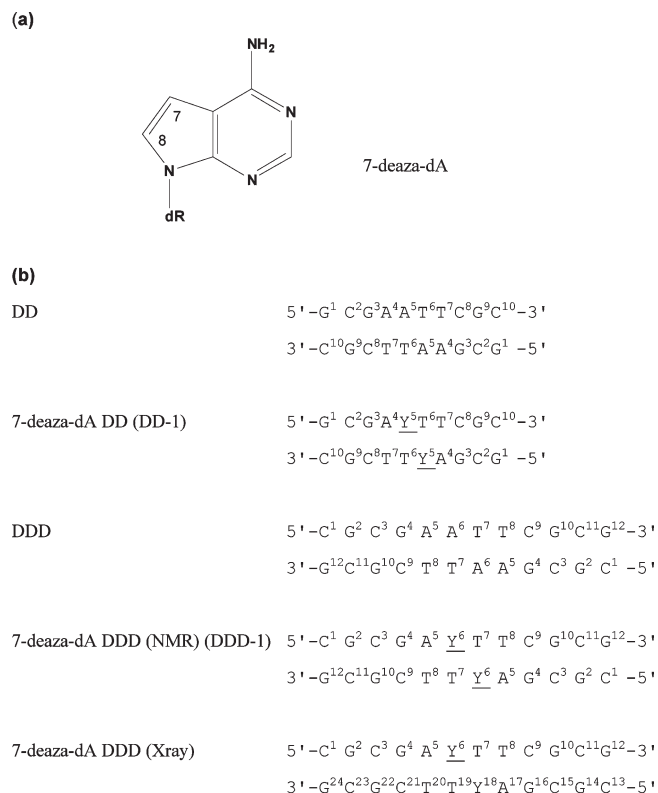
In studies presented herein, an adenine at position A⁶ in the DDD^{19,20} has been replaced by 7-deaza-dA^{15,16} to form the

Received: July 25, 2011

Revised: October 7, 2011

Published: November 08, 2011

Chart 1. (a) Structure of 7-deaza-dA and (b) Sequences and numbering of the nucleotides for unmodified DD, 7-deaza-dA DD, unmodified DDD, 7-deaza-dA DDD (NMR), and 7-deaza-dA DDD (X-ray) duplexes^a



^aIn solution, the two strands exhibit pseudo-dyad symmetry. In the crystal structure, the two strands were not symmetry related and the nucleotides were individually numbered.

DDD-1 duplex [*S'*-d(C¹G²C³G⁴A⁵Y⁶T⁷T⁸C⁹G¹⁰C¹¹G¹²)-3']₂ (Y=7-deaza-dA) (Chart 1). Crystallography has been used to determine the structure of the DDD-1 duplex. A combination of thermal melting studies monitored by UV absorbance, differential scanning calorimetry (DSC), and NMR studies have been performed. The corresponding decamer DD-1, [*S'*-d(G¹C²G³A⁴Y⁵T⁶-T⁷C⁸G⁹C¹⁰)-3']₂, which does not form an intramolecular hairpin at low salt concentrations, was also used in thermodynamic studies. We demonstrate that 7-deaza-dA has minimal effect upon base pairing geometry and conformation of the DDD. However, the 7-deaza-dA:dT base pair is thermodynamically destabilized, which is primarily attributed to unfavorable enthalpy terms dominated by less favorable stacking interactions, resulting from changes in the base electrostatics and electronic dipole–dipole interactions. There is also a net release of electrostricted waters from the duplex.

MATERIALS AND METHODS

Sample Preparation. The oligodeoxynucleotides 5'-CGCG AYTTCGCG-3' (DDD-1) and 5'-GCGAYTTCGCG-3' (DD-1), Y = 7-deaza-dA, were synthesized by the University of Nebraska Medical Center Eppley Institute Molecular Biology Shared Resource. The 7-deaza-dA phosphoramidite was obtained commercially (Glen Research, Sterling, VA, U.S.A.). The oligodeoxynucleotides were purified using semipreparative reverse-phase

HPLC (Phenomenex, Phenyl-Hexyl, 5 μ m, 250 mm \times 10.0 mm) equilibrated with 0.1 M triethylammonium acetate (pH 7.0). The unmodified oligodeoxynucleotides, 5'-CGCGAATTCGCG-3' (DDD) and 5'-GCGAATTCGCG-3' (DD), were synthesized by the Midland Reagent Company (Midland, TX) and purified by anion-exchange HPLC. The oligodeoxynucleotides were desalted using Sephadex G-25, lyophilized, and characterized by MALDI-TOF-MS. The oligodeoxynucleotides were dissolved in the appropriate buffers. The concentrations of single-stranded oligodeoxynucleotides were determined by UV absorbance at 260 nm using extinction coefficients of $1.11 \times 10^5 \text{ M}^{-1} \text{ cm}^{-1}$ (dodecamers) and $9.5 \times 10^4 \text{ M}^{-1} \text{ cm}^{-1}$ (decamers)²² and assuming similar extinction coefficients for 7-deaza-dA and dA. The oligodeoxynucleotides were annealed by heating to 80 $^\circ\text{C}$ for 15 min and then cooling to room temperature.

Temperature–Unfolding Profiles (Melting Curves). The thermodynamic parameters for the temperature-induced unfolding reactions of the duplexes were measured using a VP-DSC differential scanning calorimeter (Microcal, Inc., Northampton, MA, U.S.A.). The heat capacity profile for each DNA solution was measured against a buffer solution. The experimental curves were normalized for the heating rate, and a buffer vs buffer scan was subtracted using the program Origin (v. 5.0; Microcal, Inc.). The resulting monophasic or biphasic curves were analyzed by deconvolution with the Microcal software; their integration ($\int \Delta C_p dT$) yielded the molar unfolding enthalpy (ΔH_{cal}), which was independent of the nature of the transition.^{23,24} The molar entropy (ΔS_{cal}) was obtained similarly, using $\int (\Delta C_p/T) dT$. The free energy change at any temperature T was obtained with the Gibbs equation: $\Delta G^\circ(T) = \Delta H_{\text{cal}} - T\Delta S_{\text{cal}}$.

Absorption versus temperature profiles (UV melts) for each duplex were measured at either 260 or 275 nm using a thermoelectrically controlled UV–vis Aviv 14DS (Aviv Biomedical, Inc., Lakewood, NJ) or Lambda 40-Perkin-Elmer (Perkin-Elmer, Inc., Waltham, MA) spectrophotometers. The temperature was scanned at heating rates of 0.75–1.00 $^\circ\text{C}/\text{min}$. Melting curves as a function of strand concentration (7–70 μM) were obtained to check the molecularity of each oligodeoxynucleotide (i.e., hairpin vs duplex). Additional melting curves were obtained as a function of salt²⁵ and osmolyte concentrations^{26–28} to determine the differential binding of counterions (Δn_{Na^+}) and waters (Δn_w), which accompanied the helix-to-coil transitions.^{29,30} For duplexes that melted via biphasic transitions only the T_M of the duplex \rightarrow random coil transition was used for the calculations.

In the determination of Δn_{Na^+} , UV melts were measured in the salt range of 10–200 mM NaCl at pH 7.0, whereas in the determination of Δn_w , UV melts were measured in the ethylene glycol concentration range of 0.5–4.0 m at pH 7.0 and 10 mM NaCl. The osmolalities of the solutions were obtained with a UIC vapor pressure osmometer, Model 830 (Joliet, IL, U.S.A.). These osmolalities were then converted into water activities, a_w , using the relationship $\ln a_w = -(\text{Osm}/M_w)$, where Osm is the solution osmolality and M_w is the molality of H₂O, 55.5 mol/kg.³¹

Circular Dichroism. Circular dichroism (CD) measurements were conducted on an Aviv model 202SF CD spectropolarimeter (Aviv Biomedical, Inc., Lakewood, NJ). To approach 100% duplex formation the spectrum of each sample was obtained using a strain-free 1 cm quartz cell at low temperatures. Typically, 1 OD of a duplex DNA was dissolved in 1 mL of 10 mM sodium phosphate buffer (pH 7.0). The reported spectra correspond to an average of three scans from 220 to 350 nm at a wavelength step of 1 nm.

NMR Spectroscopy. Modified and unmodified duplexes were prepared at 0.3 mM and 1.8 mM concentrations, respectively. The samples were prepared in 10 mM NaH_2PO_4 , 0.1 M NaCl, and 50 μM Na_2EDTA (pH 7.0). The samples were exchanged with D_2O and dissolved in 0.5 mL of 99.99% D_2O to observe nonexchangeable protons. For the observation of exchangeable protons, the samples were dissolved in 0.5 mL of 9:1 $\text{H}_2\text{O}/\text{D}_2\text{O}$. ^1H NMR spectra for unmodified and modified oligodeoxynucleotides were recorded at 600 and 800 MHz. Chemical shifts were referenced to water. Data were processed using TOPSPIN software (Bruker Biospin Inc., Billerica, MA). The NOESY^{32,33} and DQF-COSY³⁴ spectra of samples in D_2O were collected at 15 °C at 800 MHz; NOESY experiments were conducted at a mixing time of 250 ms. The NOESY spectra of the modified and unmodified sample in H_2O were collected at 5 °C at 600 MHz, with a 250 ms mixing time. These experiments were performed with a relaxation delay of 2.0 s. Water suppression was performed using the WATERGATE pulse sequence.³⁵

Crystallizations and Data Collection. Crystallization trials were performed with the Nucleic Acid Mini-screen (Hampton Research, Aliso Viejo, CA).³⁶ The hanging drop vapor diffusion technique was used. Droplets, with a volume of 2 μL , of a 1:1 mixture of sample and mini-screen buffer were equilibrated against 0.75 mL of 35% 2-methyl-2,4-pentandiol (MPD) at 18 °C. The crystal used for data collection was grown in 10% MPD, 40 mM sodium cacodylate (pH 6.0), 12 mM spermine tetra-HCl, and 80 mM NaCl. The single crystal was mounted in a nylon loop and frozen in liquid nitrogen. Diffraction data were collected at low temperature in a cold nitrogen stream on beamline 21-ID-F at LS-CAT, APS (Argonne National Laboratory, Argonne, IL). Separate data sets for high and low resolution reflections were collected. All data were processed with the program HKL2000.³⁷

Crystal Structure Determination and Refinement. The diffraction data were processed in space group $P2_12_12_1$ (orthorhombic). Phasing was carried out by the molecular replacement method using the program MOLREP in the CCP4 suite.³⁸ The DDD sequence with PDB entry 355D³⁹ was used as the starting model. Initial refinements of the model were performed with the CNS program,⁴⁰ setting aside 5% randomly selected reflections for calculating the R_{free} . Rigid body refinement and simulated annealing were performed. Multiple rounds of coordinate refinements and simulated annealing led to an improved model for which sum (2Fo-Fc) and difference (Fo-Fc) Fourier electron density maps were generated. At a later stage solvent water molecules were added on the basis of Fourier 2Fo-Fc sum and Fo-Fc difference electron density maps. Water molecules were accepted based on the standard distances and B-factor criteria. Further structure refinement was performed using the program SHELX,⁴¹ and REFMAC in CCP4.³⁸ A Mg^{2+} ion and four Na^+ ions were identified in the electron density maps based on their low B-factors and the characteristic Mg^{2+} octahedral and Na^+ tetrahedral coordination geometries. Geometry and topology files were generated for the 7-deaza-dA modified bases and anisotropic temperature factor refinement was performed afterward. The program TURBO-FRODO⁴² was used to display electron density maps. The helicoidal parameters of the 7-deaza-dA-modified DDD were analyzed using the program CURVES (version 5.3).⁴³

Data Deposition. Complete structure factor and final coordinates were deposited in the Protein Data Bank (www.rcsb.org): PDB ID code 3OPI.

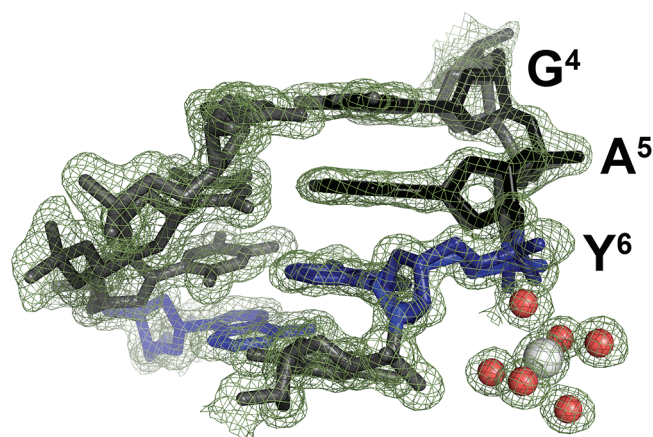


Figure 1. Sum electron density contoured at the 1.0 σ level (green meshwork) surrounding the DDD-1 duplex in the region of the G^4 , A^5 , and Y^6 nucleotides, where the phosphate groups display two alternative conformations. Bases G^4 and A^5 are shown in gray (one phosphate conformation) and black (second phosphate conformation). Modified base Y^6 is in blue (one phosphate conformation) and navy (second phosphate conformation). The Mg^{2+} ion (white sphere) is coordinated by six water molecules (red spheres). The Mg^{2+} ion interacts via coordinated waters with phosphate oxygens of one conformer of Y^6 only (second conformation of the phosphate backbone is shown in navy) and T^7 residue. Similar interactions are observed in the unmodified DDD duplex (PDB entry 355D). This interaction does not involve the N7 atom of Y^6 and is maintained for the 7-deaza-dA base.

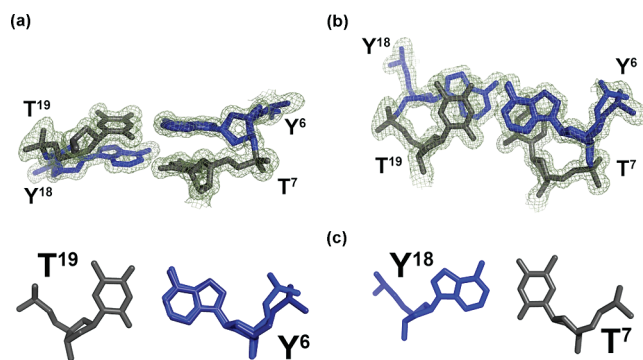


Figure 2. Sum electron density contoured at the 1.0 σ level (green meshwork) around the modified Y^6 , T^{19} and Y^{18} , T^7 along the normal to the base pairs, viewed (a) from the side and (b) from the top approximately the named to base pairs, revealing stacking interactions. (c) Watson–Crick base pairing of 7-deaza-dA · dT. Y^6 and Y^{18} bases are shown in blue.

RESULTS

Crystallography. The 7-deaza-dA-modified DDD-1 diffracted at a resolution of 1.1 Å. The two strands of the DDD-1 duplex were not symmetry-related in the crystal. Therefore, each of the nucleotides was uniquely numbered (Chart 1). Minimal perturbation of the DNA duplex was observed at the 7-deaza-dA site (Figure 1).⁴⁴ The 7-deaza-dA bases were in the *anti* conformation about the glycosyl bonds and Watson–Crick base pairing was maintained at base pairs $\text{Y}^6 \cdot \text{T}^{19}$ and $\text{Y}^{18} \cdot \text{T}^7$ (Figure 2). Waters formed the anticipated minor groove inner spine of hydration (Figure S1 of the Supporting Information), similar to the situation in the DDD.^{19,20,44} The replacement of N7-dA with a carbon atom in 7-deaza-dA⁶ did not alter Mg^{2+} binding in

Table 1. Crystal Data, Data Collection, and Refinement Statistics

space group	orthorhombic $P2_12_12_1$
cell parameters (Å)	$a = 25.64$, $b = 40.31$, $c = 65.93$
temperature of data collection (°C)	-170
wavelength (Å)	0.9785
max resolution (Å)	1.1
unique reflections	27920
completeness all/ 1.14–1.10 Å (%)	97.8/95.8
redundancy all/ 1.14–1.1 Å	10.6/6.9
$I/\sigma(I)$ all/ 1.14–1.1 Å	61.26/4.8
R_{merge} all/ 1.14–1.10 Å	0.048/0.394
R_{work}	0.161
R_{free}	0.195
number of DNA atoms	486
number of water molecules	133
number of ions	1 Mg^{2+} 4 Na^+
rms distances (Å)	0.024
rms angles (°)	1.95

the crystal, e.g., as indicated by a comparison to the high resolution structure of the DDD obtained by Tereshko and Egli.⁴⁴ One Mg^{2+} ion was present per asymmetric unit, but two Mg^{2+} ions interacted with each DNA molecule as a consequence of the crystallographic 2_1 symmetry. This Mg^{2+} interacted via six coordinated waters with the G^2 and G^{22} nucleotides in the major groove (Figure 1). It also interacted via coordinated waters with the Y^6 and T^7 phosphate oxygens from an adjacent DNA molecule. It did not interact directly with the Y^6 7-deaza-dA base (Figure 1; Figure S2 of the Supporting Information). Instead, it stabilized a contact between DNA molecules. The sum electron density contoured at the 1.0 σ level for the G^4 , A^5 and Y^6 nucleotides suggested two conformations of the phosphate backbone (Figure S2 of the Supporting Information). These were each refined with occupancy 0.5. It is likely that these were due to this Mg^{2+} -mediated lattice contact between DNA molecules. Helicoidal analyses indicated that the rise, roll, and twist parameters of the DDD-1 duplex were unaffected by these two backbone conformations (Figure S3 of the Supporting Information). The difference between the two conformations primarily involved torsion angle α (S' -P-O-CS-C4-3') (Figure S4 of the Supporting Information). Smaller variations were observed in other torsion and glycosyl angles of the G^4 , A^5 and Y^6 nucleotides (Figure S5 of the Supporting Information). In all, 133 waters and four Na^+ ions, of which one was observed at the S' -ApT-3' step,⁴⁴ were assigned per asymmetric unit. A summary of crystal data and data collection statistics is given in Table 1.

Circular Dichroism. The CD spectra of the DDD and DDD-1 dodecamers are shown in Figure 3. These experiments were performed at 16 mM $[\text{Na}^+]$. In both instances, a positive Cotton effect was observed, centered near 280 nm. In both instances, a negative Cotton effect was centered at 250 nm. These were characteristic of a right-handed helix in the B-DNA family. There was an 18% decrease in the intensity of the 250 nm band for DDD-1 relative to DDD. CD experiments with the decamers DD and DD-1 revealed a similar trend. The decreased intensity of the 250 nm band for DD-1 relative to DD was 10% (Figure 3).

NMR Spectroscopy. In solution, the pseudodyad symmetry of the DNA duplex results in the symmetry-related resonances from

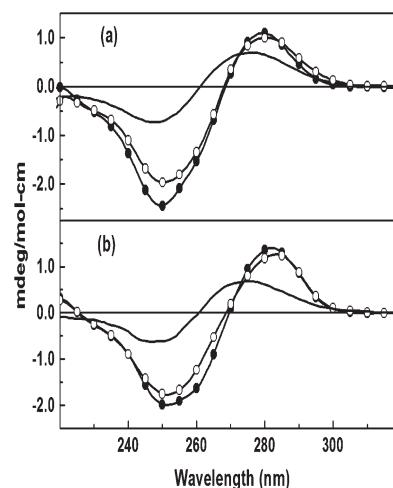


Figure 3. CD spectra of duplexes in 10 mM sodium phosphate buffer (pH 7.0) at 4 °C, $\sim 10 \mu\text{M}$ strand concentration: (a) DDD (●) and DDD-1 (○) and (b) DD (●) and DD-1 (○). The spectra without symbols are the spectra of the unmodified DDD and DD at 90 °C.

the two strands being isochronous;^{45,46} thus, the NMR resonances are labeled for nucleotides 1–12. The 7-deaza-dA H7 and H8 protons were assigned from a combination of COSY and NOESY spectra, which established the presence of the 7-deaza-dA base at position Y^6 in the DDD-1 duplex (Figure S6 in the Supporting Information). The upfield chemical shift of 1.07 ppm observed for Y^6 H8 relative to A^6 H8 in the DDD was attributed primarily to different electron distributions in the pyrrolopyrimidine vs purine bases, not to a conformational change in the DDD-1 duplex. The nonexchangeable DNA protons were assigned using standard methods.^{47,48} All sequential NOEs between the aromatic and anomeric protons of the DDD-1 duplex were observed (Figure S6 in the Supporting Information). The imino proton region of the NOESY spectrum of the DDD-1 duplex is shown in Figure 4. The sequential connectivity of the base imino protons was obtained from base pairs $\text{G}^2 \cdot \text{C}^{11} \rightarrow \text{C}^3 \cdot \text{G}^{10} \rightarrow \text{G}^4 \cdot \text{C}^9 \rightarrow \text{A}^5 \cdot \text{T}^8 \rightarrow \text{Y}^6 \cdot \text{T}^7$.⁴⁹ Cross peaks from A^5 H2 to T^8 N3H and Y^6 H2 to T^7 N3H were observed. For the imino protons, the greatest downfield shift of 0.49 ppm was observed for the T^7 imino proton. The imino resonances of the terminal base pairs $\text{C}^1 \cdot \text{G}^{12}$ were missing. This was attributed to rapid exchange with water.

Unfolding Studies. (a). *NMR.* Spectra of the DDD-1 and DDD duplexes were collected as a function of temperature, over the range 5–65 °C (Figure 5). At 15 °C, for the 7-deaza-dA-modified duplex, the T^7 imino resonance began to broaden, compared with the other peaks and with the unmodified DDD. At 45 °C, the T^7 peak completely broadened. These observations indicated that the T^7 imino proton was in enhanced exchange with the solvent and indicated a destabilization of the $\text{Y}^6 \cdot \text{T}^7$ base pair.

(b). *UV Melting Studies.* The unfolding of duplexes was studied by temperature-dependent UV spectroscopy. Absorption spectra at low and high temperatures revealed a greater hyperchromic effect at 260 nm for DDD and DD and at 275 nm for DDD-1 and DD-1. These were chosen as optimum wavelengths used for all UV melting studies. Typical melting curves of dodecamer and decamer duplexes are shown in Figure 6. In 10 mM NaCl, dodecamers (DDD and DDD-1) unfolded in broad biphasic transitions, whereas decamers (DD and DD-1)

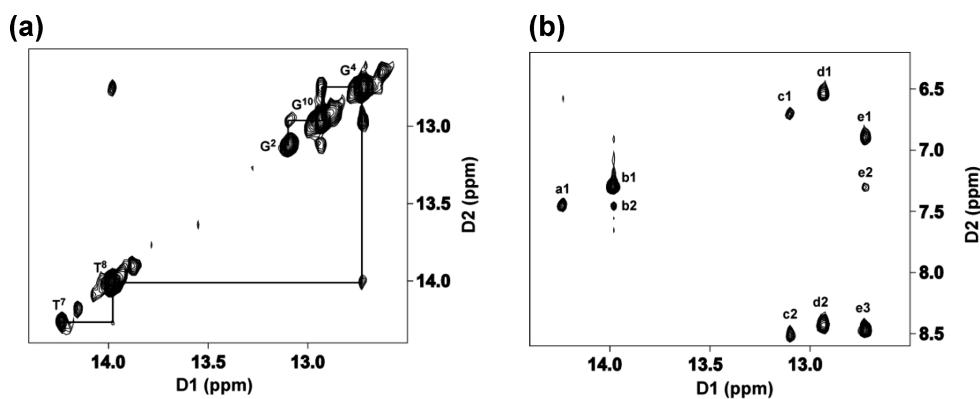


Figure 4. (a) NOE connectivity for the imino protons for the base pairs $G^2 \cdot C^{11}$ to $Y^6 \cdot T^7$. The experiments were carried out at a mixing time of 250 ms and 600 MHz at 5 °C. (b) Interstrand NOE cross peaks between opposite bases: a1, $T^7 N^3 H \rightarrow Y^6 H^2$; b1, $T^8 N^3 H \rightarrow A^5 H^2$; b2, $T^8 N^3 H \rightarrow Y^6 H^2$; c1, $G^2 N^1 H \rightarrow C^{11} N^2 H^2$; c2, $G^2 N^1 H \rightarrow C^{11} N^2 H^1$; d1, $G^{10} N^1 H \rightarrow C^3 N^2 H^2$; d2, $G^{10} N^1 H \rightarrow C^3 N^2 H^1$; e1, $G^4 N^1 H \rightarrow C^9 N^2 H^2$; e2, $G^4 N^1 H \rightarrow A^5 H^2$; e3, $G^4 N^1 H \rightarrow C^9 N^2 H^1$.

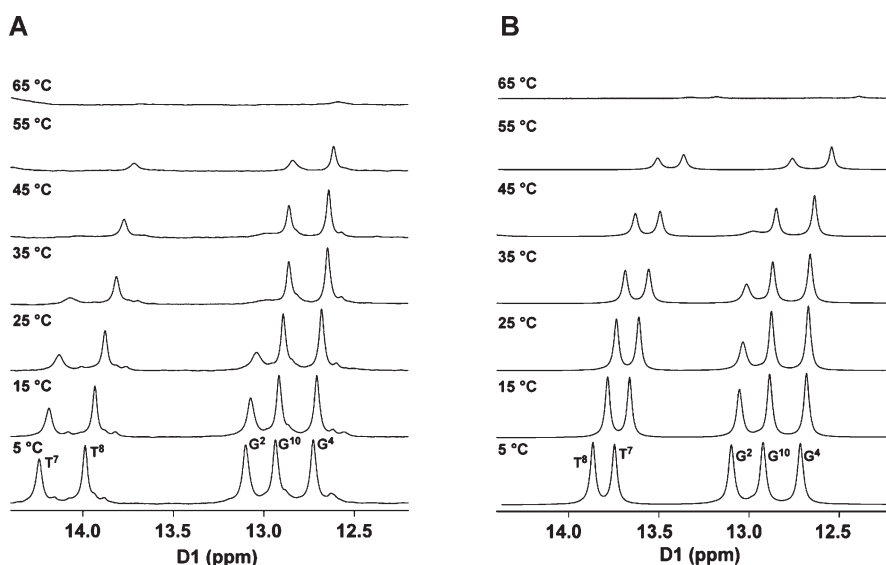


Figure 5. ^1H NMR of imino proton resonances as a function of temperature. (A) 7-deaza-dA DDD-1 duplex. (B) Unmodified DDD duplex. Modified and unmodified duplexes were prepared at 0.3 mM and 1.8 mM concentration respectively. The samples were prepared in 10 mM NaH_2PO_4 , 0.1 M NaCl, and 50 μM Na_2EDTA at pH 7.0.

unfolded via monophasic transitions. The overall sequential melting behavior corresponded to duplex \rightarrow hairpin and hairpin \rightarrow random coil transitions, while the corresponding dodecamers, which formed less stable hairpins, melted through a single duplex random coil transition. The T_M values were determined by taking the first derivative of the melting curves, and shape analysis of these curves are reported in Table 2. Incorporation of 7-deaza-dA was destabilizing for both dodecamer and decamer. The T_M of the first transition for the dodecamer DDD-1 relative to DDD was unchanged in 16 mM Na^+ (low salt) and 8.2 °C lower in 116 mM Na^+ (high salt) concentrations. At higher salt concentration both melting transitions overlapped and only one transition was observed. The T_M of the modified DD-1 was lower than that for DD by 3.4 °C in low salt and by 5.5 °C in high salt.

DSC of the 7-Deaza-dA-Modified Duplexes. The DSC melting curves for the DDD and DDD-1 dodecamers and the DD and DD-1 decamers are shown in Figure 7, and the thermodynamic profiles are listed in Table 2. At the lower salt concentration

(16 mM Na^+), the helix–coil transition was biphasic for the dodecamers. The DDD unfolded via a broad first transition and a sharper second transition. The biphasic DSC thermogram of DDD-1 revealed a broad peak with a shoulder for the first transition at lower temperature that could not be resolved. At increased salt concentration, the dodecamers unfolded via monophasic transitions. This was attributed to higher screening by salt on the duplex phosphates, relative to the phosphates of the hairpin. This shifts the duplex transition to higher temperatures, confirming the helix \rightarrow hairpin \rightarrow random coil transitions of each dodecamer duplex, which was observed in the UV melting studies. For the decamers, the helix–coil transitions were monophasic, confirming their unfolding through a duplex to random coil transition as seen in the UV studies. Enthalpies were determined by deconvolution of the DSC graphs; however, only the model-independent enthalpies of the duplex \rightarrow random coil transitions are reported in Table 2. The dA to 7-deaza-dA substitution was destabilizing at both low and high salt concentrations.

Analysis of thermograms of dodecamers revealed decreased endothermic enthalpies of 40.0 and 35.5 kcal/mol for DDD-1 relative to DDD in 10 and 100 mM NaCl, respectively (Table 3). For decamers, endothermic enthalpies of 80.1 kcal/mol for DD and a reduced unfolding enthalpy of 56.4 kcal/mol for DD-1 (Table 3) were obtained at low salt. At the higher salt concentration, the $\Delta\Delta H$ was 18.2 kcal/mol for DD vs DD-1.

Thermodynamic Profiles for the Formation of Each Duplex. The thermodynamic data is provided in Table 2. The favorable Gibbs free energies, indicating spontaneous formation of each duplex, resulted from compensation of favorable enthalpy and unfavorable entropy contributions. The favorable enthalpies arose from the formation of base pairs and base pair stacks, uptake of electrostricted waters, and release of structural waters, whereas the unfavorable entropy terms included the ordering of two strands to form a duplex, condensation of counterions, and immobilization of waters.

Relative to the unmodified oligodeoxynucleotides, the 7-deaza-dA modified oligodeoxynucleotides were destabilized at low and high salt concentrations. The inclusion of two 7-deaza-dA modifications in DDD-1 yielded a decrease in ΔG of 2.3 and 5.1 kcal/mol in 10 and 100 mM NaCl, respectively, whereas in

decamers ΔG decreases of 1.8 and 2.5 kcal/mol in low and high salt, respectively, were observed following two 7-deaza-dA substitutions.

Differential Association of Water Molecules. T_M dependencies on water activity were studied to determine the thermodynamic association of water molecules to DNA duplexes. By increasing concentrations of the osmolyte ethylene glycol from 0.5 to 4.0 m the activity of water was decreased. The UV melting curves showed that the T_M s of the dodecamers (DDD and DDD-1) and decamers (DD and DD-1) decreased linearly with increasing osmolyte concentrations (i.e., decreasing activity of water). The T_M dependence on water activity of dodecamers and decamers are shown in Figure 8. The slopes of these lines, $\partial T_M / \partial \log a_w$, in conjunction with the $\Delta H / RT_M^2$ term, were used to obtain the differential association of water molecules. The Δn_w values for the formation of each duplex in 10 mM NaCl are shown in Table 2. Water uptake values, expressed as mol H₂O per mol duplex, measured in low salt, were 38 (DDD) and 19 (DDD-1) for dodecamers, and 30 (DD) and 17 (DD-1) for decamers. At the higher salt concentration (116 mM Na⁺), Δn_w values followed a similar trend. Lower Δn_w values at this salt concentration (Table 2) were due to increased screening of the water dipoles at higher salt concentration. The overall effect, and assuming that the random coil states of all the duplexes behave similarly at higher temperature, was that the substitution of

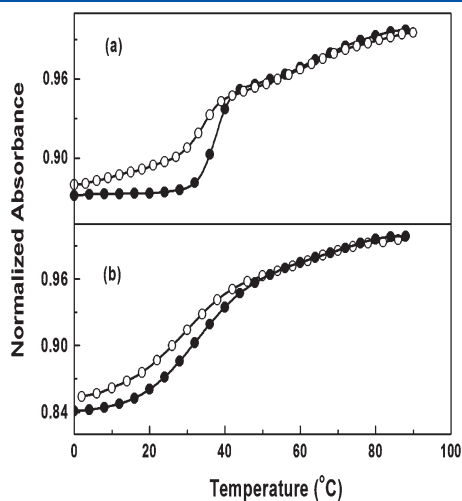


Figure 6. UV melting curves in 10 mM sodium phosphate buffer (pH 7.0) $\sim 40 \mu\text{M}$ total strand concentration for (a) DDD (●) at 260 nm and DDD-1 (○) at 275 nm and (b) DD (●) at 260 nm and DD-1 (○) at 275 nm.

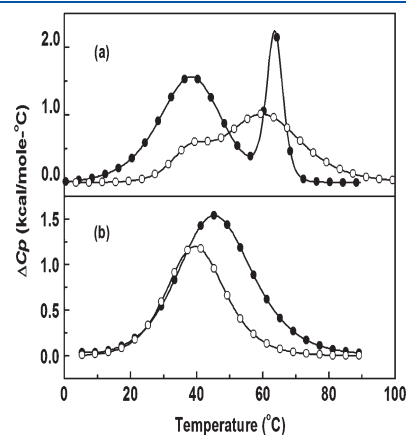


Figure 7. DSC curves in 10 mM sodium phosphate buffer (pH 7.0): (a) DDD (●) and DDD-1 (○) at $\sim 200 \mu\text{M}$ and (b) DD (●) and DD-1 (○) at $\sim 300 \mu\text{M}$.

Table 2. Thermodynamic Profiles for the Formation of Duplexes at 20 °C.^a

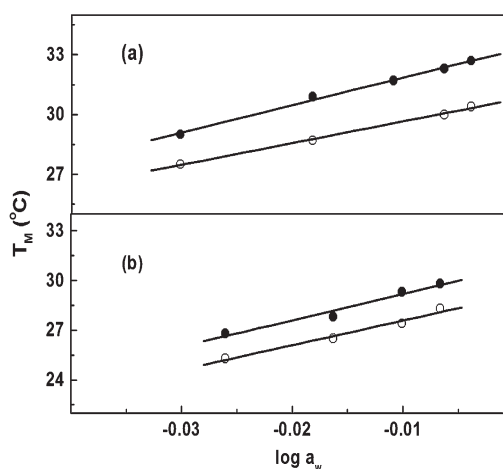
oligodeoxynucleotide	NaCl ^b	T_M ^c	ΔG° ^{d,e}	ΔH° ^e	$T\Delta S^\circ$	Δn_{Na^+} ^f	Δn_w ^f
DDD	10	33.3	-6.9	-116.0	-109.1	-2.3 ± 0.2	-38.0 ± 2.0
	100	57.7	-15.5	-109.5	-94.0	-1.8 ± 0.1	-30.0 ± 2.0
DDD-1	10	34.5	-4.6	-76.0	-71.4	-1.4 ± 0.1	-19.0 ± 2.0
	100	49.5	-10.4	-74.0	-63.6	-1.1 ± 0.1	-15.0 ± 2.0
DD	10	29.5	-5.6	-80.1	-74.5	-2.2 ± 0.2	-30.0 ± 4.0
	100	53.0	-8.2	-72.3	-64.1	-1.7 ± 0.1	-22.0 ± 3.0
DD-1	10	26.1	-3.8	-56.4	-52.6	-1.5 ± 0.2	-17.0 ± 2.0
	100	47.5	-5.7	-54.1	-48.4	-1.3 ± 0.1	-14.0 ± 2.0

^a Parameters are measured from UV (T_M) and DSC melting curves in 10 mM sodium phosphate buffer (pH 7.0). The observed standard deviations are T_M (± 0.5), ΔH_{cal} ($\pm 3\%$), ΔG_{20} ($\pm 5\%$), and $T\Delta S_{\text{cal}}$ ($\pm 3\%$). ^b Salt concentration in mM. ^c °C. ^d Determined at 20 °C. ^e kcal/mol. ^f Per mol DNA. Δn_{Na^+} was determined experimentally, using the linking number: $\Delta n_{\text{Na}^+} = \partial \ln K / \partial \ln [\text{Na}^+]$, where K corresponds to two single strands in equilibrium with a duplex.

Table 3. Differential Thermodynamic Profiles for Pairs of Dodecamer and Decamer Duplexes

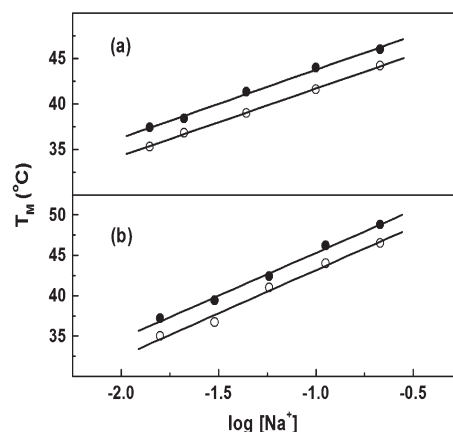
NaCl ^a	$\Delta\Delta H^c$	$\Delta\Delta G^{o,b,c}$	$\Delta(T\Delta S)^c$	$\Delta\Delta n_{\text{Na}^+}^d$	$\Delta\Delta n_w^d$
Substitution of dA ⁶ with 7-Deaza-dA in DDD (DDD-1 Minus DDD)					
10	40.0	2.3	37.7	0.9	19.0
100	35.5	5.1	30.4	0.7	15.0
Substitution of dA ⁵ with 7-Deaza-dA in DD (DD-1 Minus DD)					
10	23.7	1.8	21.9	0.7	13.0
100	18.2	2.5	15.7	0.4	8.0

^a Salt concentration in mM. ^b Determined at 20 °C. ^c kcal/mol. ^d Per mol DNA.

**Figure 8.** T_M dependence on osmolyte concentration (as a function of ethylene glycol) for duplexes in 10 mM sodium phosphate buffer (pH 7.0), $\sim 5 \mu\text{M}$ strand concentration for (a) DDD (●) and DDD-1 (○) and $\sim 7 \mu\text{M}$ strand concentration for (b) DD (●) and DD-1 (○).

7-deaza-dA into duplex DNA caused a decreased association of water molecules. For instance, there was a $\Delta\Delta n_w$ of 19 and 15 between DDD and DDD-1 at 10 mM and 100 mM NaCl, respectively, and $\Delta\Delta n_w$ of 13 and 8 between the pair of decamer duplexes at low and high salt, respectively (Table 3). Parameters used to calculate differential water binding for dodecamers are shown in Table S1 in the Supporting Information.

Differential Association of Counterions. UV melting curves at salt concentrations ranging from 16 to 216 mM $[\text{Na}^+]$ were measured to examine the thermodynamic association of counterions with the DNA duplexes. The T_M values of the DDD and DDD-1 dodecamers, and DD and DD-1 decamers increased linearly with salt concentration (Figure 9), consistent with the expectation that the duplex states should have higher charge density parameters. The T_M dependence on salt concentration for dodecamers and decamers are shown in Figure 9, panels a and b, respectively. The slopes of these lines, $\partial T_M / \partial \log[\text{Na}^+]$, in conjunction with the experimentally determined $\Delta H/RT_M^2$ terms, allowed measurement of differential counterion binding. The Δn_{Na^+} values for the formation of each duplex, from the association of two complementary strands, in low and high salt are shown in Table 2. In low salt, the Na^+ uptake as measured in mol Na^+ per mol duplex was 2.3 for the DDD dodecamer and 1.4 for the DDD-1 dodecamer, and 2.2 for the DD dodecamer and 1.5 for the DD-1 decamer. The Δn_{Na^+} values at the higher salt concentration of

**Figure 9.** T_M dependencies on salt concentration for duplexes in 10 mM sodium phosphate buffer (pH 7.0), $\sim 5 \mu\text{M}$ strand concentration for (a) DDD (●) and DDD-1 (○) and $\sim 7 \mu\text{M}$ strand concentration for (b) DD (●) and DD-1 (○).

116 mM showed a similar trend; however, the values were lower due to the higher screening of the phosphates by salt (Table 2). The average differential Na^+ uptake as measured in mol Na^+ per mol phosphate was estimated as 0.094 (DDD and DD) in this range of salt concentration, which was consistent with the fact that these oligodeoxynucleotides were not behaving electrostatically as long polyelectrolytes.⁵⁰ However, the main effect, assuming that the random coil states of the different single strand oligodeoxynucleotides were thermodynamically similar at higher temperatures, was that the introduction of 7-deaza-dA into the duplex DNA caused a slightly decreased association of counterions. For instance, there was a $\Delta\Delta n_{\text{Na}^+}$ of 0.9 and 0.7 between DDD and DDD-1 at 10 and 100 mM NaCl, respectively, and $\Delta\Delta n_{\text{Na}^+}$ of 0.7 and 0.4 between the pair of decamer duplexes at low and high salt, respectively (Table 3). Parameters used to calculate differential counterion binding for dodecamers are presented in Table S2 in the Supporting Information.

DISCUSSION

It has been assumed that 7-deaza-dA, an isostere for dA in duplex DNA, does not substantially perturb the duplex, and thus provides a good model for dA. However, in light of suggestions that 7-deaza-dA introduces a large structural perturbation to the B-form of poly(dA-dT)·poly(dA-dT),¹⁸ it was of interest to provide a comprehensive characterization of B-DNA with a 7-deaza-dA modification. The Dickerson–Drew dodecamer^{19,20} provides a well-characterized system suitable for detailed crystallographic analysis,⁴⁴ as well as NMR analysis.^{46,51,52} The present studies provide the first high-resolution crystallographic data for the substitution of adenine with 7-deaza-dA in duplex DNA.

Structure of the 7-Deaza-dA:dT Base Pair. The structure of the 7-deaza-dA:dT base pair in the DDD duplex reveals that 7-deaza-dA has minimal effect on duplex conformation (Figure 1) and base pair geometry (Figure 2) as compared to a canonical dA:dT base pair. Substitution of 7-deaza-dA changes the electronegative N7-dA atom to a carbon atom, which alters the electrostatics of the nucleobase. Consistent with this expectation, the downfield shift of the T⁷ imino resonance (Figure 5) is attributed to stronger hydrogen bonding with the more electronegative 7-deaza-dA N1 nitrogen. Thus, the observed destabilization of 7-deaza-dA does not result from a decrease in H-bonding but

must be due to other changes induced by the perturbation of the electrostatic potential in the major groove. Other NMR chemical shift perturbations are minimal, which indicates that the modification does not affect the structure at the flanking nucleotides. Our results differ from those of Pope et al.,¹⁸ who suggested that replacement of dA by 7-deaza-dA caused perturbations to B-DNA for the poly[d(7-deaza-dA-T)]·poly[d(7-deaza-dA-T)] duplex. The physical properties of poly(dA-dT) differ from the DDD, and it may be of interest to look for structural perturbations induced by 7-deaza-dA in other sequences.

7-Deaza-dA Enthalpically Destabilizes the DDD. The 7-deaza-dA substitution thermodynamically destabilizes the DDD-1 and DD-1 duplexes, compared to the unmodified DDD and DD duplexes. This is evidenced by the $\Delta\Delta G$ values (computed as the average of 10 and 100 mM $[\text{Na}^+]$, Table 3). At 20 °C, $\Delta\Delta G$ is decreased by 3.7 kcal/mol for DDD-1 and by 2.2 kcal/mol for DD-1. In both cases, the major contributor to the reduced $\Delta\Delta G$ values is the enthalpy term, which drops 37.8 kcal/mol for DDD-1 and 20.9 kcal/mol for DD-1 (Table 3). The differential $\Delta\Delta H$ values at different salt concentrations suggest the presence of heat capacity effects. The heat capacity values were 0.8 kcal/K mol (DDD) and -0.08 kcal/K mol (DDD-1), and -0.5 kcal/K mol (DD) and -0.2 kcal/K mol (DD-1). These may be due to exposures of nonpolar groups to solvent and/or to changes in structural hydration between the random coil and duplex states of DDD-1 and DD-1.⁵³ The present data lead to a different conclusion than did studies of (7-deaza-dA)₁₁A·T₁₂ as compared to dA₁₂·dT₁₂, conducted by Seela and Thomas.¹⁷ They concluded that destabilization induced by 7-deaza-dA was minimal and was associated with an unfavorable entropy change.¹⁷ It should be noted, however, that the DDD presents a different sequence context than does the A-tract dA₁₂·dT₁₂ sequence.⁵⁴

Base Stacking Effects. The most significant contribution to the unfavorable $\Delta\Delta H$ term (Table 3) of 32.7 kcal/mol for DDD-1 (17.6 kcal/mol for DD-1) results from a reduction of stacking enthalpy in the modified duplexes, attributed to less favorable π – π interactions involving the pyrrolopyrimidine ring of 7-deaza-dA and the neighboring base pairs vs adenine. In the CD spectra, the intensities of the negative bands near 250 nm are thought to track base stacking contributions. The band intensities at 250 nm are consistent with reduced base stacking in DDD-1 and DD-1 at low temperature (Figure 3). There is an 18% decrease in the intensity of the 250 nm band for DDD-1 relative to DDD. The decreased intensity of the 250 nm band for DD-1 relative to DD is 10%. However, changes in the electronic structure of 7-deaza-dA may modulate the relative optical dipole orientations responsible for the CD bands. Exchange-mediated line broadening of DNA imino protons is often associated with the rate-limiting formation of an open state of the base pair in which the imino proton is freed from its hydrogen bond and is accessible to the base that catalyzes the proton exchange.^{55–59} The increased broadening of the Y⁶·T⁷ base pair thymine N3 imino resonance (Figure 5) is consistent with this model, which correlates with reduced stacking enthalpy of the DDD-1 duplex relative to the DDD duplex. However, the possibility that base pair opening is not rate-limiting cannot be ruled out, with the line broadening reflecting a more rapid hydrogen exchange catalysis for the substituted duplex.⁶⁰ In this regard, the C7–H on the 7-deaza-dA (as compared to the: N7 on the natural dA) would be anticipated to exhibit a reduced electrostatic repulsion with hydroxide or phosphate base catalyst.

Duplex Hydration. The unfavorable $\Delta\Delta H$ term observed upon incorporation of 7-deaza-dA is partially attributed to reduced hydration of the modified duplexes. This may, in part, be due to the more hydrophobic major groove edge of 7-deaza-dA as compared to dA. Thus, 7-deaza-dA substitution results in a $\Delta\Delta n_w$ of 17 H₂O per mol DNA for DDD-1 and 11 H₂O per mol DNA for DD-1 (obtained by averaging the data obtained in 10 and 100 mM NaCl, Table 3). This “translates” into a reduction of approximately 9 H₂O per mol DNA per 7-deaza-dA nucleotide for the DDD-1 duplex and 6 H₂O per mol DNA per 7-deaza-dA nucleotide for the DD-1 duplex, assuming localized effects. A release of 17 water molecules from the DDD-1 duplex (11 water molecules from the DD-1) accounts for an unfavorable enthalpy term $\Delta\Delta H$ of 5.1 kcal/mol (3.3 kcal/mol for the DD-1).⁶¹ The release of waters indicates increases in the volumes of the modified systems, i.e., positive $\Delta\Delta V$ terms. Since $\Delta\Delta G$ is also positive, this indicates release of electrostricted waters from DDD-1 and DD-1.⁶² There may also be a compensating increase of structural water due to the more hydrophobic major groove edge of 7-deaza-dA. Another way to interpret the data is that the displacement of water by ethylene glycol, used in the osmotic stress experiments, near 7-deaza-dA will be more facile than at dA because of the reduced electrostatic interaction with solvent. In any case, similar reductions in hydration were observed for DNA modified with 7-deaza-dG nucleotides.⁷

Cation Binding. The introduction of the 7-deaza-dA:dT pair into the DDD causes a decrease in the differential association of cations. This is reflected in the $\Delta\Delta n_{\text{Na}^+}$ of 0.9 and 0.7 between DDD and DDD-1 at 10 and 100 mM NaCl, respectively, and $\Delta\Delta n_{\text{Na}^+}$ of 0.7 and 0.4 between the pair of decamer duplexes at low and high salt, respectively. The reduced uptake of Na⁺ is not attributed to the loss of a major groove high affinity cation binding site near the 7-deaza-dA nucleotide. High-resolution crystallographic structures of the DDD^{19,20} provide insight into the sequence-dependent distribution of waters and counterions in B-DNA.^{39,44,63–72} When the DDD was crystallized in the presence of Tl⁺, no high-occupancy cation binding sites were observed in the major groove near A⁶. Likewise, Tereshko and Egli⁴⁴ did not observe a high affinity cation site near A⁶. In the present crystallographic unit cell two Mg²⁺ ions interact with the DNA, but they are not associated with the major groove edge of either Y⁶ or Y¹⁸ (Figure 1; Figure S2 in the Supporting Information). This is consistent with the notion that cation binding in A-T tracts occurs in the minor groove.⁶⁸ It seems possible that the thermodynamically measured decrease in the association of cations could be due to the disruption of non-specific cation binding, particularly in the minor groove. In any case, the contribution to the large $\Delta\Delta H$ term for the release of counterions is anticipated to be negligible since counterion release contributes predominantly to the $\Delta(T\Delta S)$ term.⁷³ In contrast, the major groove high-affinity cation sites in the DDD were associated with the major groove edge of dG nucleotides.⁶⁹ Indeed, the incorporation of 7-deaza-dG into the DDD was accompanied by changes in hydration and major groove cation organization.⁷

Summary. Introduction of the 7-deaza-dA:T base pair into the DDD has minimal effect upon base pairing geometry and DNA conformation, as evidenced by a combination of crystallographic and NMR studies. The 7-deaza-dA retains Watson–Crick hydrogen bonding, but the 7-deaza-dA:dT base pair is thermodynamically destabilized. A detailed analysis reveals that this is due to primarily to unfavorable enthalpy terms, which are dominated by less favorable

stacking interactions, resulting from changes in the base electrostatics and electronic dipole–dipole interactions. There is also a net release of electrostricted waters from the duplex. The introduction of the 7-deaza-dA:dT pair into the DDD causes a decreased association of cations, which is reflected in the $T\Delta S$ term.

■ ASSOCIATED CONTENT

S Supporting Information. The Supporting Information includes Tables S1, parameters used to calculate differential counterion binding for the dodecamers; S2, parameters used to calculate differential water binding for dodecamers; and Figures S1, stick model and electron density of the crystal structure of 7-deaza-dA modified DDD-1; S2, interactions between Mg^{2+} ion and DDD-1 duplex; S3, interbase pair parameters (helical rise, roll, twist); S4, comparison of backbone torsion angles (alpha and beta) of DDD and DDD-1; S5, comparison of gamma, delta, epsilon, chi and zeta angles in the crystal structures of the DDD-1; S6, expanded plots of NOESY spectrum of the DDD-1 duplex showing sequential NOEs between the aromatic and anomeric protons and COSY spectrum. This material is available free charge via the Internet at <http://pubs.acs.org>.

■ AUTHOR INFORMATION

Corresponding Author

*Telephone: 615-322-2589. Fax: 615-322-7591. E-mail: michael.p.stone@vanderbilt.edu.

■ ACKNOWLEDGMENT

This work was supported by NIH Grant R01 GM68430 (L.A.M., M.P.S., and B.G.) and R01 GM055237 (M.E.). Funding for the NMR spectrometers was supplied by Vanderbilt University and by NIH Grant RR-05805. Vanderbilt University and the Vanderbilt Center for Structural Biology assisted with the purchase of in-house crystallographic instrumentation. Crystallographic data were collected on the 21-ID-F beamline of the Life Sciences Collaborative Access Team (LS-CAT) at the Advanced Photon Source (Argonne National Laboratory, Argonne, IL). Supporting institutions may be found at <http://ls-cat.org/members.html>. Use of the Advanced Photon Source was supported by the U.S. Department of Energy, Basic Energy Sciences, Office of Science, under Contract W-31109-Eng-38.

■ REFERENCES

- (1) Suhadolnik, R. J. *Nucleoside Antibiotics*; Wiley-Interscience: New York, 1970.
- (2) Smulson, M. E.; Suhadolnik, R. J. *J. Biol. Chem.* **1967**, *242*, 2872–2876.
- (3) Mizusawa, S.; Nishimura, S.; Seela, F. *Nucleic Acids Res.* **1986**, *14*, 1319–1324.
- (4) Malygin, E. G.; Zinoviev, V. V.; Petrov, N. A.; Evdokimov, A. A.; Jen-Jacobson, L.; Kossykh, V. G.; Hattman, S. *Nucleic Acids Res.* **1999**, *27*, 1135–1144.
- (5) Shchyolkina, A. K.; Kaluzhny, D. N.; Arndt-Jovin, D. J.; Jovin, T. M.; Zhurkin, V. B. *Nucleic Acids Res.* **2006**, *34*, 3239–3245.
- (6) Ramzaeva, N.; Michalek, E.; Kazimierczuk, Z.; Seela, F.; Rosemeyer, H. *Chem. Biodivers.* **2007**, *4*, 2725–2744.
- (7) Ganguly, M.; Wang, F.; Kaushik, M.; Stone, M. P.; Marky, L. A.; Gold, B. *Nucleic Acids Res.* **2007**, *35*, 6181–6195.
- (8) Gold, B.; Marky, L. M.; Stone, M. P.; Williams, L. D. *Chem. Res. Toxicol.* **2006**, *19*, 1402–1414.

- (9) Anzai, K.; Nakamura, G.; Suzuki, S. *J. Antibiot. (Tokyo)* **1957**, *10*, 201–204.
- (10) McCarty, R. M.; Bandarian, V. *Chem. Biol.* **2008**, *15*, 790–798.
- (11) McCarty, R. M.; Somogyi, A.; Lin, G.; Jacobsen, N. E.; Bandarian, V. *Biochemistry* **2009**, *48*, 3847–3852.
- (12) Ono, A.; Ohtani, Y.; Sato, M.; Ueda, T. *Nucleic Acids Symp. Ser.* **1983**, 67–70.
- (13) Seela, F.; Berg, H.; Rosemeyer, H. *Biochemistry* **1989**, *28*, 6193–6198.
- (14) Seela, F.; Grein, T. *Nucleic Acids Res.* **1992**, *20*, 2297–2306.
- (15) Seela, F.; Kehne, A. *Tetrahedron* **1985**, *41*, 5387–5392.
- (16) Seela, F.; Ramzaeva, N.; Leonard, P.; Chen, Y.; Debelak, H.; Feiling, E.; Kroschel, R.; Zulauf, M.; Wenzel, T.; Frohlich, T.; et al. *Nucleosides Nucleotides Nucleic Acids* **2001**, *20*, 1421–1424.
- (17) Seela, F.; Thomas, H. *Helv. Chim. Acta* **1995**, *78*, 94–108.
- (18) Pope, L. H.; Shotton, M. W.; Forsyth, T.; Hughes, D. J.; Denny, R. C.; Fuller, W. *Biophys. Chem.* **1998**, *70*, 161–172.
- (19) Wing, R.; Drew, H.; Takano, T.; Broka, C.; Tanaka, S.; Itakura, K.; Dickerson, R. E. *Nature* **1980**, *287*, 755–758.
- (20) Drew, H. R.; Wing, R. M.; Takano, T.; Broka, C.; Tanaka, S.; Itakura, K.; Dickerson, R. E. *Proc. Natl. Acad. Sci. U.S.A.* **1981**, *78*, 2179–2183.
- (21) Wang, F.; Li, F.; Ganguly, M.; Marky, L. A.; Gold, B.; Egli, M.; Stone, M. P. *Biochemistry* **2008**, *27*, 7147–7157.
- (22) Cavaluzzi, M. J.; Borer, P. N. *Nucleic Acids Res.* **2004**, *32*, e13.
- (23) Marky, L. A.; Breslauer, K. J. *Biopolymers* **1987**, *26*, 1601–1620.
- (24) Rentzeperis, D.; Marky, L. A.; Dwyer, T. J.; Geierstanger, B. H.; Pelton, J. G.; Wemmer, D. E. *Biochemistry* **1995**, *34*, 2937–2945.
- (25) Chaires, J. B. *Biopolymers* **1985**, *24*, 403–419.
- (26) Spink, C. H.; Chaires, J. B. *Biochemistry* **1999**, *38*, 496–508.
- (27) Qu, X.; Chaires, J. B. *J. Am. Chem. Soc.* **2001**, *123*, 1–7.
- (28) Yu, H.; Ren, J.; Chaires, J. B.; Qu, X. *J. Med. Chem.* **2008**, *51*, 5909–5911.
- (29) Cantor, C. R.; Schimmel, P. R. *Biophysical Chemistry*; Freeman: San Francisco, 1980.
- (30) Kaushik, M.; Suehl, N.; Marky, L. A. *Biophys. Chem.* **2007**, *126*, 154–164.
- (31) Courtenay, E. S.; Capp, M. W.; Anderson, C. F.; Record, M. T., Jr. *Biochemistry* **2000**, *39*, 4455–4471.
- (32) Jeener, J.; Meier, B. H.; Bachmann, P.; Ernst, R. R. *J. Chem. Phys.* **1979**, *71*, 4546–4553.
- (33) Wagner, R.; Berger, S. *J. Magn. Res. A* **1996**, *123*, 119–121.
- (34) Piantini, U.; Sorensen, O. W.; Ernst, R. R. *J. Am. Chem. Soc.* **1982**, *104*, 6800–6801.
- (35) Piotto, M.; Saudek, V.; Sklenar, V. *J. Biomol. NMR* **1992**, *6*, 661–665.
- (36) Berger, I.; Kang, C. H.; Sinha, N.; Wolters, M.; Rich, A. *Acta Crystallogr. D* **1996**, *52*, 465–468.
- (37) Otwinowski, Z.; Minor, W. *Acta Crystallogr. A* **1997**, *276*, 307–326.
- (38) Collaborative Computational Project Number 4 *Acta Crystallogr. D* **1994**, *50*, 760–763.
- (39) Shui, X.; McFail-Isom, L.; Hu, G. G.; Williams, L. D. *Biochemistry* **1998**, *37*, 8341–8355.
- (40) Brunger, A. T.; Adams, P. D.; Clore, G. M.; DeLano, W. L.; Gros, P.; Grosse-Kunstleve, R. W.; Jiang, J. S.; Kuszewski, J.; Nilges, M.; Pannu, N. S.; et al. *Acta Crystallogr. D* **1998**, *54*, 905–921.
- (41) Sheldrick, G. M.; Schneider, T. R. *Methods Enzymol.* **1997**, *277*, 319–343.
- (42) Cambillau, C.; Roussel, A. 1997, Université Aix-Marseille II, Marseille, France.
- (43) Ravishankar, G.; Swaminathan, S.; Beveridge, D. L.; Lavery, R.; Sklenar, H. *J. Biomol. Struct. Dyn.* **1989**, *6*, 669–699.
- (44) Tereshko, V.; Minasov, G.; Egli, M. *J. Am. Chem. Soc.* **1999**, *121*, 470–471.
- (45) Pardi, A.; Tinoco, L., Jr. *Biochemistry* **1982**, *21*, 4686–4693.
- (46) Hare, D. R.; Wemmer, D. E.; Chou, S. H.; Drobny, G.; Reid, B. R. *J. Mol. Biol.* **1983**, *171*, 319–336.

- (47) Reid, B. R. *Q. Rev. Biophys.* **1987**, *20*, 2–28.
- (48) Patel, D. J.; Shapiro, L.; Hare, D. *Q. Rev. Biophys.* **1987**, *20*, 35–112.
- (49) Boelens, R.; Scheek, R. M.; Dijkstra, K.; Kaptein, R. *J. Magn. Reson.* **1985**, *62*, 378–386.
- (50) Hud, N. V. 2009, In *Nucleic Acid-Metal Ion Interactions*; Hud, N. V., Ed.; RSC Publishing: Cambridge, UK.
- (51) Pardi, A.; Morden, K. M.; Patel, D. J.; Tinoco, I., Jr. *Biochemistry* **1982**, *21*, 6567–6574.
- (52) Tjandra, N.; Tate, S.; Ono, A.; Kainosho, M.; Bax, A. *J. Am. Chem. Soc.* **2000**, *122*, 6190–6200.
- (53) Makhataдзе, G. I.; Privalov, P. L. *J. Mol. Biol.* **1990**, *213*, 375–384.
- (54) Hagerman, P. J. *Nature* **1986**, *321*, 449–450.
- (55) Teitelbaum, H.; Englander, S. W. *J. Mol. Biol.* **1975**, *92*, 79–92.
- (56) Mandal, C.; Kallenbach, N. R.; Englander, S. W. *J. Mol. Biol.* **1979**, *135*, 391–411.
- (57) Englander, S. W.; Kallenbach, N. R. *Q. Rev. Biophys.* **1984**, *16*, 521–655.
- (58) Leroy, J. L.; Kochoyan, M.; Huynh-Dinh, T.; Gueron, M. *J. Mol. Biol.* **1988**, *200*, 223–238.
- (59) Folta-Stogniew, E.; Russu, I. M. *Biochemistry* **1996**, *35*, 8439–8449.
- (60) Benight, A. S.; Schurr, J. M.; Flynn, P. F.; Reid, B. R.; Wemmer, D. E. *J. Mol. Biol.* **1988**, *200*, 377–399.
- (61) Gasan, A. I.; Maleev, V. Y.; Semenov, M. A. *Stud Biophys* **1990**, *136*, 171–178.
- (62) Marky, L. A.; Kupke, D. W. *Methods Enzymol.* **2000**, *323*, 419–441.
- (63) Egli, M.; Tereshko, V.; Teplova, M.; Minasov, G.; Joachimiak, A.; Sanishvili, R.; Weeks, C. M.; Miller, R.; Maier, M. A.; An, H.; Dan Cook, P.; Manoharan, M. *Biopolymers* **1998**, *48*, 234–252.
- (64) Shui, X.; Sines, C. C.; McFail-Isom, L.; VanDerveer, D.; Williams, L. D. *Biochemistry* **1998**, *37*, 16877–16887.
- (65) Minasov, G.; Tereshko, V.; Egli, M. *J. Mol. Biol.* **1999**, *291*, 83–99.
- (66) McFail-Isom, L.; Sines, C. C.; Williams, L. D. *Curr. Opin. Struct. Biol.* **1999**, *9*, 298–304.
- (67) Williams, L. D.; Maher, L. J., III. *Annu. Rev. Biophys. Biomol. Struct.* **2000**, *29*, 497–521.
- (68) Woods, K. K.; McFail-Isom, L.; Sines, C. C.; Howerton, S. B.; Stephens, R. K.; Williams, L. D. *J. Am. Chem. Soc.* **2000**, *122*, 1546–1547.
- (69) Howerton, S. B.; Sines, C. C.; VanDerveer, D.; Williams, L. D. *Biochemistry* **2001**, *40*, 10023–10031.
- (70) Egli, M. *Chem. Biol.* **2002**, *9*, 277–286.
- (71) Woods, K. K.; Lan, T.; McLaughlin, L. W.; Williams, L. D. *Nucleic Acids Res.* **2003**, *31*, 1536–1540.
- (72) Egli, M.; Tereshko, V. *ACS Symp. Ser.* **2004**, *884*, 87–109.
- (73) Krakauer, H. *Biopolymers* **1972**, *11*, 811–828.